Research Article | Vol. 26, No. 21 | 15 Oct 2018 | OPTICS EXPRESS 26961
Optics EXPRESS

Auto-alignment of X-ray focusing mirrors with speckle-based at-wavelength metrology

TUNHE ZHOU, HONGCHANG WANG,* OLIVER FOX, AND KAWAL SAWHNEY

Diamond Light Source Ltd, Harwell Science and Innovation Campus, Didcot OX11 0DE, UK
**hongchang.wang@diamond.ac.uk*

Abstract: Significant improvements have been made in the fabrication of diffraction-limited X-ray optics used to pursue an aberration-free wavefront. Alignment of these optics plays a crucial role in the resultant beam quality. Here, we present a simple and fast alignment method based on imaging X-ray near-field speckle patterns, with experimental demonstration using a pair of Kirkpatrick-Baez mirrors. The proposed technique has the potential to be an alternative to conventional methods. It loosens the stringent demand for high-resolution scanning stages compared to conventional knife-edge scan and, hence, can be applied to nano-focusing optics. The flexibility and straightforward implementation of the method allow it to be applied to a wide range of experiments at synchrotron facilities and laboratory-based sources.

Published by The Optical Society under the terms of the Creative Commons Attribution 4.0 License. Further distribution of this work must maintain attribution to the author(s) and the published article's title, journal citation, and DOI.

1. Introduction

Experiments at modern synchrotron radiation sources are becoming increasingly sophisticated to probe the smallest scale of structures in materials. This places stringent demands on wavefront quality and, therefore, the performance of the X-ray optics employed on the beamlines. X-ray mirrors operating at grazing angle are one type of optics commonly used for focusing or collimating X-ray beams with high efficiency. A Kirkpatrick-Baez (KB) pair is a typical arrangement used to form a point focus by having separate horizontal and vertical line focusing mirrors [1]. When aiming to achieve an aberration-free wavefront with optics produced with highly accurate fabrication processes, *in situ* alignment plays an important role attaining the best possible performance. A misaligned optical system can induce wavefront aberration or enlarged focal spot sizes that degrade the image quality or lower the flux intensity for beamline experiments.

The most common way to align KB mirrors is to use a trial and error method, evaluating the focal spot size or wavefront aberration as a feedback. With advanced fabrication techniques, KB mirrors can achieve nano-focusing [2], which cannot be resolved directly by current X-ray scintillator-based detectors. Knife-edge fluorescent or wire-absorption scans using photodiode detectors [3, 4] also face challenges due to the requirement for nanometer resolution on the translation mechanism. Employing a tilted stripe mask has been proposed as an alternative to knife-edge fluorescence measurements by scanning the mask along beam propagation direction rather than orthogonally across the beam, and thereby reducing the need for such precise translation stages [5]. However, the alignment is more complicated and it requires an accurate tilt stage and a sophisticated periodic mask. The scan is still time-consuming because it is one-dimensional (1D) whereas the focus needs to be found in three-dimensional (3D) space. Wavefront sensing, for example using a Hartmann sensor or shearing interferometry [6, 7], can give two-dimensional (2D) information directly. Hartmann and Shack-Hartmann sensing applied in X-ray regime have been mostly used for soft X-rays [8–10] and has been recently extended to hard X-rays as well [11, 12] with advantage of single-shot ability but low spatial resolution. Shearing interferometry with either double or single

#337773 https://doi.org/10.1364/OE.26.026961
Journal © 2018 Received 4 Jul 2018; revised 9 Sep 2018; accepted 9 Sep 2018; published 1 Oct 2018

Optics EXPRESS

grating system has been widely used in the last decade in the hard X-ray range [7, 13, 14], for which the fabrication of nearly perfect gratings is however not trivial. Recently, ptychography has seen rapid progress due to its ability to quantitatively retrieve the whole beam profile from optics to image plane and, therefore, the focal plane can be determined and the wavefront aberration characterized simultaneously [15]. It has great potential but is currently still challenging to apply on partially coherent sources, such as bending magnet beamlines and laboratory sources. Large numbers of scans (typically a few hundred [16]) are required for successful retrieval of phase information, which can make it time-consuming.

To overcome these limitations, we present a simple approach for aligning KB mirrors developed from a speckle-based technique [17]. Easily accessible materials are used to generate speckle patterns as a wavefront mask [18, 19]. Images acquired by an area detector provide information in 3D space that can be used to locate the focal position in an efficient way. The requirements for the scanning stage resolution and mechanical stability are significantly relaxed, allowing accurate results under flexible experimental conditions. With the proposed method, the mirror alignment procedure is simplified, and a fast auto-alignment system can be realized.

2. Methods

As illustrated in Fig. 1(a), an ideal mirror is an arc of an ellipse with semi-major axis a and semi-minor axis b. A ray from a point source at distance p with incident angle θ gets reflected by the mirror and focuses at distance q. The curvature of the mirror surface is

$$k = \frac{\sin\theta(p+q)}{2pq} \approx \frac{\theta}{2q} \tag{1}$$

where θ is assumed to be small and p is much larger than q [20]. This shows that for a mirror with fixed surface curvature, the change of incident angle is approximately proportional to the change of focal length as

$$\Delta\theta/\theta_0 \approx \Delta q/q_0 \tag{2}$$

where θ_0 and q_0 are the designed values for the center of the mirror. Equation (1) can also be expressed in the Cartesian coordinates (x,y) of the ellipse as

$$\Delta q(x) \approx \frac{\Delta\theta}{2k(x)} = \Delta\theta \cdot \frac{1}{2ab}\left(a^2 - \frac{a^2-b^2}{a^2}x^2\right)^{\frac{3}{2}} \tag{3}$$

which shows that only $\Delta\theta = 0$ can give a constant q that is not dependent on x [21].

To measure Δq and realize $\Delta\theta = 0$ experimentally, the speckle-based metrology technique is proposed. The principle of the technique was previously described in detail in [17] and is illustrated here in Fig. 1. The principle of the speckle-based technique is essentially similar to other wavefront sensing methods [6, 7], but with a different wavefront modulator. A piece of sandpaper is used as the static diffuser to generate speckle patterns as a wavefront mask. An area detector situated downstream records a stack of images while the diffuser is scanned across the beam. The distance from the focus to the detector plane R_i for pixel i can be calculated with the proportionality relation

$$\frac{R_i}{R_i - L} = \frac{d(i-j)}{s_i} \tag{4}$$

where L is the distance between the diffuser and the detector, d is the detector pixel size, i and j are the indices of two chosen rows on the detector, and s is the corresponding distance on the diffuser plane between the rays that are incident on pixels in rows i and j. Assuming the

Optics EXPRESS

diffuser is scanned linearly with a step size η, two speckle patterns can be constructed from rows i and j in the stack of images from the scan, as shown in Fig. 1(b). Using cross correlation [22], the linear translation ξ between the two patterns can be calculated, and the distance of the two rays on the diffuser plane is then equivalent to the displacement of the diffuser where $s_i = \xi_i \eta$.

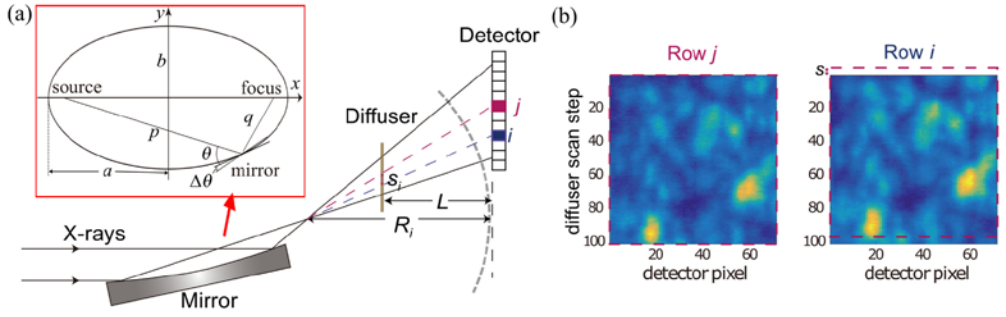

Fig. 1. Principle of the speckle-based technique for mirror metrology: (a) illustration of the experimental alignment with inset showing the geometrical design of an elliptical mirror; (b) example of two speckle patterns taken from two different rows, from which displacement can be clearly observed.

Although developed from a wavefront sensing technique, the proposed method for mirror alignment functions more similar to the slit-scan technique [23, 24] by retrieving the ray aberration from the distorted focus. For simplicity, the discussion here only considers one mirror in one dimension because the KB mirrors can be decoupled as two line focusing mirrors. Using the definition of wavefront aberration as the optical path difference between the geometrical wavefront and the ideal wavefront [25], ΔR (difference between aberrated and ideal) is used to characterize the wavefront aberration. The final aberration δ_t is a combination resulting from several uncorrelated errors, including from alignment error δ_a, the mirror height error δ_m and from upstream optics δ_u

$$\delta_t^2 = \delta_a^2 + \delta_m^2 + \delta_u^2. \tag{5}$$

We assume that the quality of the mirror and the upstream wavefront is good enough so that the dominant error derives from the misalignment $\delta_t^2 \approx \delta_a^2$. When the mirror is well aligned, rays reflected from an ideal mirror surface onto the detector should diverge from the same focal point to a perfect spherical wavefront with $R_i = R_0$. If the pitch of the mirror is misaligned, tilt aberration and coma will occur [26], and R_i will vary for different pixel positions, as shown in Fig. 2(a), derived from numerical simulations based on geometrical ray tracing [20]. This can be combined with Eq. (3) under the small angle assumption so that $\Delta R \approx -\Delta q$. Practically, it is difficult to accurately calculate the discrete value of $k(x)$ in real world coordinates, so one of the most common mathematical treatments is to use polynomial fitting for calibration of aberrations [27], which we adapt here for R_i as

$$R_i = P_0 + P_1 i + \cdots + P_n i^n. \tag{6}$$

As expected from Eq. (3), the polynomial coefficients exhibit a linear relationship with the misalignment angle $\Delta\theta$ in simulations, as shown in Fig. 2(b). First order is used here for calibration given by

$$P_1(\theta) = \alpha_1 \Delta\theta = \alpha_1 \theta + \alpha_0 \tag{7}$$

Optics EXPRESS

where α_0 and α_1 can be found by linear fitting. Therefore, the alignment is optimized when $\Delta\theta = 0$ and $P_1 = 0$.

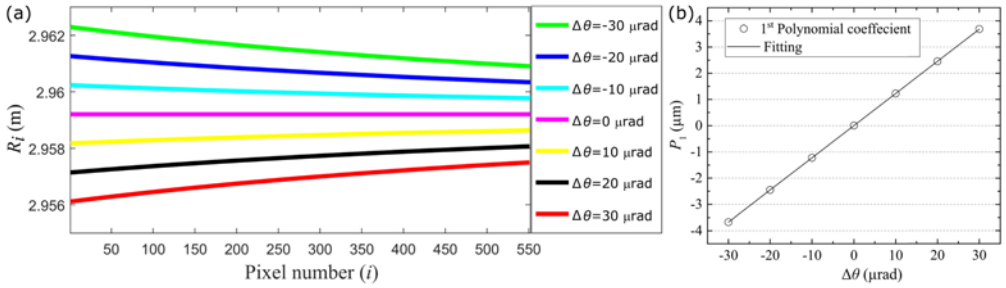

Fig. 2. (a) Simulated R_i at different tilt angles along the detector. (b) The 1st order polynomial coefficient P_1 varies linearly with tilt angle and is equal to 0 when incident angle is correctly aligned.

The average of R_i over all pixels i is also found to have a linear relationship with $\Delta\theta$ from the simulation given by

$$\overline{R}(\theta) = R_0 + \beta_1 \Delta\theta = \beta_1 \cdot \theta + \beta_0 \tag{8}$$

which agrees with the theoretical approximation in Eq. (2). The coefficients in Eq. (8) β_0 and β_1 can be found experimentally during the alignment process and, hence, the focus can be located for any angle.

3. Experiments

3.1. Parameters

The proposed method was applied experimentally for alignment of a KB mirror system at the B16 Test Beamline at the Diamond Light Source [28]. The X-ray energy was 15 keV, selected by a double crystal monochromator. The KB system consisted of two elliptical mirrors with designed parameters of {p_h = 45.11 m, q_h = 0.125 m, θ_h = 3 mrad} for the horizontal focusing mirror (HFM) and {p_v = 45 m, q_v = 0.235 m, θ_v = 3 mrad} for the vertical focusing mirror (VFM). The mirror system was mounted on a motorized tower with 6 degrees of freedom (Kohzu Precision Co. Ltd.), located ~46 m from the bending magnet source. The mirrors were manually aligned to be parallel to the beam using X-ray radiography and the initial angle set to 0 mrad before they were tilted by 3 mrad to match the designed incident angle. The wavefront modulator was a piece of sandpaper with 5 μm silicon carbide grains, mounted on a 2D piezo stage (Physik Instrumente Ltd.). The detector was a scintillator-based charge-coupled device (CCD) camera with a pixel size of 6.45 μm (Photonic Science Ltd.), placed ~3 m downstream of the mirror. Vertical and horizontal gold-wire knife-edges were also mounted close to the estimated focal position to allow comparison with the speckle-based method. A passivated implanted planar silicon diode detector was mounted further downstream to measure the wire scanning signal. During the experiments the pitch angle of the mirror was changed with a 10 μrad step size around the initial position. At each pitch angle, a 1D speckle scan was performed with a 200 nm step size, a scan range of 20 μm and a detector exposure time of 5 s.

3.2. Results and discussion

Experimental results from aligning the pitch angles of the KB mirror pair are shown in Fig. 3, where the 1st polynomial coefficient P_1 (squares) and $\overline{R}$ (circles) are plotted with respect to pitch angle. The linear fit, as described in Eqs. (7) and (8), is plotted as solid lines and the coefficients and root mean square (RMS) residual of the fitting are given in Table 1. The

Optics EXPRESS

negative value for the HFM angle results from the definition of the stage axes during the experiment. Whether the slope of P_1 and $\overline{R}$ was positive or negative depended on how the pitch angle and the detector pixel index were defined, and does not affect the calculation of the correct angle for alignment. The experimental results are in good agreement with simulations, as shown in Table 1, which indicates that the assumption that the misalignment error dominants the wavefront error is valid in this case. It also means that a simulation can be used as an aid in the alignment procedure for verification and to reduce the number of data points required for a sufficient fitting. Compared to the theoretical approximation in Eq. (2), which gives $\beta_{1,v}$ = 78.33 and $\beta_{1,h}$ = 41.66, the experimental results are also broadly similar. However, there is still a small difference between the theoretical values and the numerical simulations, which means that, although the theoretical approximation can be used as a guide for alignment, a more accurate alignment technique is still necessary.

From the results in Table 1, we find that when $P_1 = 0$, $\theta_{v,a}$ = 3.0120 mrad for the VFM and $\theta_{h,a}$ = –2.9675 mrad for the HFM, and differ from the initial alignment values of $\theta_{v,1}$ = 3 mrad and $\theta_{h,1}$ = –3 mrad for the VFM and HFM, respectively. From the fitting results for $\overline{R}$, the astigmatism between the focus of the VFM and the HFM at the original alignment $\theta_{v/h,1}$ was 1.86 mm (indicated in Fig. 3 by the dash-dot lines). Whereas, the astigmatism for $\theta_{v/h,a}$ is calculated to be 0.275 mm and, therefore, is significantly reduced at the aligned position. The VFM or HFM can be moved along beam propagation direction to reduce the astigmatism even more. The distance from the focus to the diffuser can also be calculated, which means that, for dedicated microscopic, diffraction or fluorescent imaging experiments, the diffuser can be mounted on the sample stage and the sample translated exactly to the focal plane determined by the speckle-based alignment.

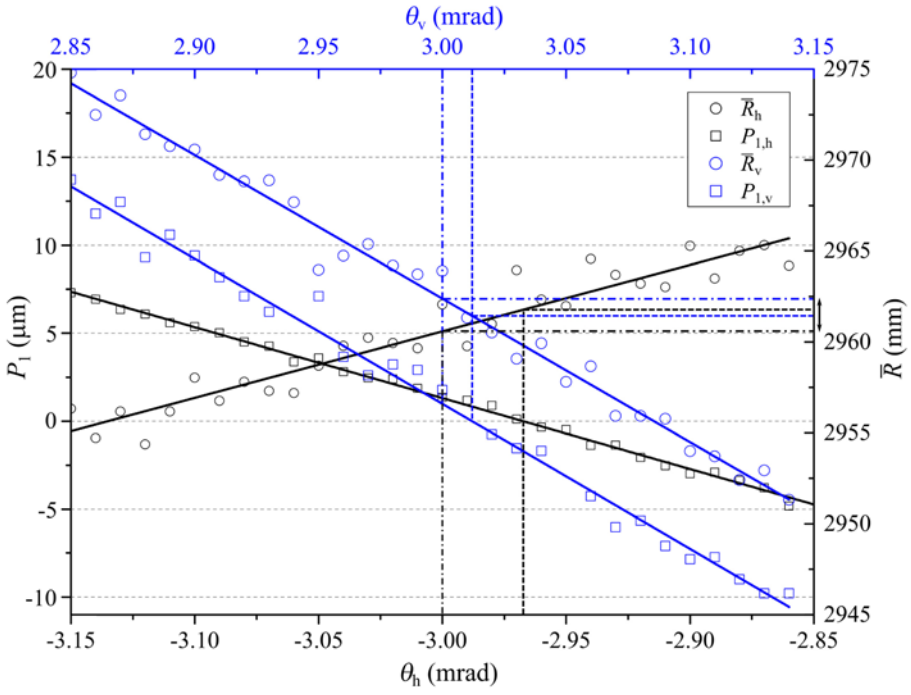

Fig. 3. Experimentally determined 1st-polynomial coefficient P_1 and $\overline{R}$ as a function of pitch angle for the KB mirror pair.

Optics EXPRESS

Table 1. Experimental results of linear fitting according to Eqs. (7) and (8) and comparison with simulated values.

Fitting results		P_1			$\overline{R}$		
		α_1	α_0	RMS	β_1	β_0	RMS
VFM	Experiment	–82.38	248.13	0.76	–78.93	3199.2	0.61
	Simulation	–82.90			–76.85		
	Difference	0.6%			2.7%		
HFM	Experiment	–40.28	–119.53	0.21	36.55	3070.2	0.95
	Simulation	–39.45			38.17		
	Difference	2.1%			4.2%		

Additionally, the speckled-based method can provide 2D information about the focusing optic [29]. The 2D measurement of $\overline{R}$ with the median value removed is shown in Fig. 4(a) and 4(b) at angles of θ_v = 2.85 mrad and θ_v = 3 mrad, respectively. The butterfly-like patterns are due to radiation damage of the mirror surface from previous white beam experiments and masked out for the following analysis. The horizontal stripe patterns are mainly due to the slope error of the mirror surface, which can also be seen in the inset in Fig. 6 and in previous studies [30]. Zernike polynomial fitting [31] was applied on ΔR and the first 7 coefficients, representing tilt, defocus, astigmatism and coma, are shown in Fig. 4(c). Higher-order terms are not calculated as they are more easily affected by the mid-frequency slope error or defects of the mirror and are also not necessary for guidance of the alignment. The significant change in the vertical tilt (2nd Zernike coefficient) between the two pitch angles, indicated by the arrow in Fig. 4(c), is expected from the 1D result shown in Fig. 3. For line focusing optics like in this demonstration, the 1D treatment provides sufficient information for alignment to remove tilt aberration and is computationally much faster.

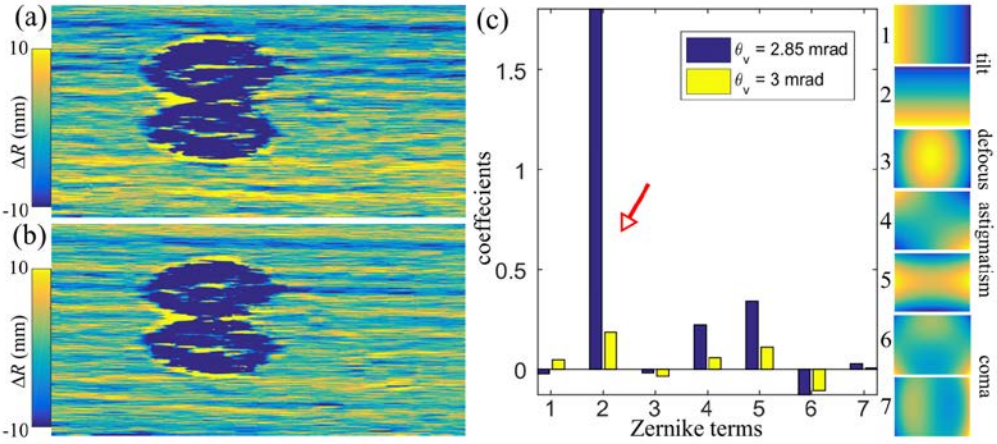

Fig. 4. Experimentally determined ΔR in 2D at (a) θ_v = 2.85 mrad and (b) θ_v = 3 mrad. (c) Zernike polynomial coefficients of the first 7 terms for which the classical names and the images of the polynomials are listed on the righthand side.

For comparison, conventional wire scanning was also conducted to align the KB mirrors. A 200 μm diameter gold-wire was scanned across the reflected beam as a knife edge. The derivative of the measured intensity was fitted with a Gaussian function and the full width at half maximum (FWHM) was used as measure of the beam size. The scan was carried out at different positions along the beam propagation direction z for both the VFM and HFM at two different pitch angles (Fig. 5). The appearance of more noise in the measurement of the VFM (black lines) than for the HFM (blue lines) is partly due to smaller numerical aperture for the VFM, which results in a wider depth of focus. Greater mechanical vibration in vertical direction from the wire mounting stages also contributes to the higher noise in the

Optics EXPRESS

measurement of the VFM, which is especially pronounced around the focus between z = 0.5 mm and 2.5 mm at $\theta_{v,1}$ (dashed black line). This variability demonstrates the limitations of the wire scanning approach that requires higher mechanical and thermal stability to achieve accurate results. Although it is not possible to obtain accurate focus positions from the wire scanning result, we can see that the focal plane of the VFM (Fig. 5) is shifted by ~3 mm between $\theta_{v,1}$ and $\theta_{v,2}$ and agrees with the value calculated from the speckle-based measurements in Table 2. For the HFM, the shift of the focal plane between $\theta_{h,1}$ and $\theta_{h,2}$ is calculated to be 0.8 mm from the speckle-based methods (Table 2), but about 0.4 mm by wire-scanning methods (Fig. 5). The difference is likely to be due to the coarse step size of the wire translation in z. The 0.2 mm wire thickness also introduces some error into the calculation of the focal plane position, especially for the HFM, which has a larger numerical aperture and narrower depth of focus. For the initial angles $\theta_{v/h,1}$, the astigmatism between the VFM and HFM is ~2 mm, which agrees with the calculations from the speckle measurement (Table 2 and Fig. 3). For the second angle $\theta_{v/h,2}$ the alignment was improved in the aspect of significantly reduced astigmatism. The second alignment by the wire scanning method demonstrates a situation which is often regarded as an optimized alignment on beamline experiments. This is because undertaking a 3D wire scan is often too time-consuming and the technique does not have enough sensitivity to detect the small beam size variations required to achieve an optimized focus. With proposed technique applied, the false optimization with only astigmatism removed will no longer be an issue.

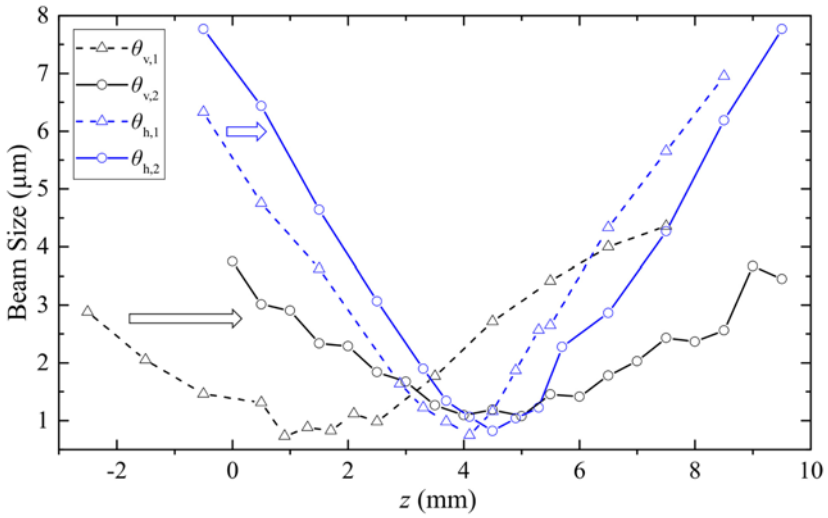

Fig. 5. Measured beam size determined by wire scanning for the VFM and HFM at the initial alignment angle $\theta_{v/h,1}$ and at a second test angle $\theta_{v/h,2}$.

Table 2. Calculated $\overline{R}$ for two different pitch angles derived from speckle-based methods.

	θ_v	$\overline{R}_v$	θ_h	$\overline{R}_h$
1	3 mrad	2962.4 mm	–3 mrad	2960.6 mm
2	3.0424 mrad	2959.1 mm	–3.0195 mrad	2959.8 mm

The error in the proposed speckle-based method is a combined contribution of cross-correlation error, the systematic error from mechanical and thermal instability, and the measurement error of the distance L. The error from cross-correlation is related to exposure time, subset window size and speckle visibility [32, 33]. It is calculated in this experiment by setting $i = j$ which gives an RMS error of 0.3%. A realistic estimation of error derived from

Optics EXPRESS

stability tests on B16 beamline was given by the sum of vibrations from all stages and was in the range of ~10 nm. However, because each cross-correlation calculation used a 2D map consisting of 100 steps, the error is decreased by an order of magnitude and, hence, ~0.5% for a 200 nm step size. With its high accuracy, the speckled-based method proposed has also proven useful for testing the stability and repeatability of the mechanical system employed for mounting mirrors over a long period of time.

The dominant error in the calcluation of $\overline{R}$ derives from the manual measurement of the distance L. However, it does not affect the alignment of the mirrors because the constant L has no influence when calculating $P_1(\theta) = 0$ in Eq. (7). Experimentally the measurement of L can be improved by using an accurate laser system or by repeating the experiments at multiple distances to minimize the error. Assuming a measurement error e, we have $L = L_m + e$, where L_m is the measured distance. Substituting it into Eq. (4) and replacing the pixel dependent variables with their averages gives

$$L_m = \overline{R}\left[1 - \frac{\bar{s}}{d(i-j)}\right] - e. \tag{9}$$

A linear fit can then be applied to calculate $\overline{R}$ and e if the relative distances between each L_m are known, which is possible with an accurate translation stage. This is shown in Fig. 6, where one speckle-based scan was taken at 6 diffuser positions at 50 mm spacing. The inset in Fig. 6 shows the retrieved speckle pattern displacement ξ_i between 2 rows of pixels in the detector plane. The oscillation of ξ_i is mainly due to the mirror slope error [30], where similar characteristics are observed for all the diffuser positions. The higher value and amplitude for larger ξ_i is due to the higher angular sensitivity from the smaller effective scanning steps with larger magnification. The linear fit according to Eq. (9) has a residual RMS of 1.53 mm and Pearson's correlation coefficient of 0.9998. The standard error of the fitting result of $\overline{R}$ is 0.9%. The values from fitting can be used in the alignment or other experiments that require the distance between the diffuser plane and the detector plane to be calculated accurately.

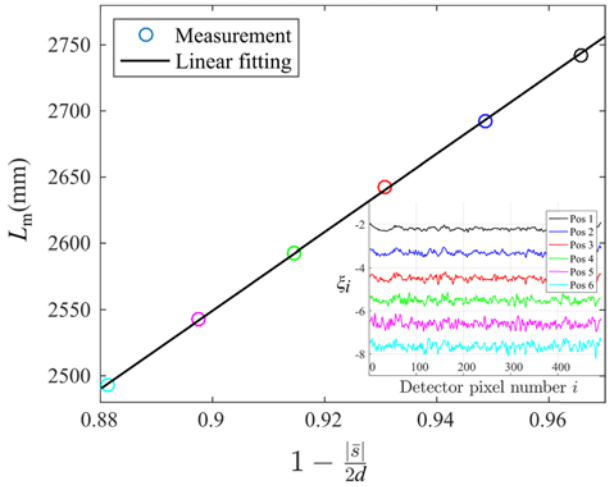

Fig. 6. Linear fit of measurements at 6 diffuser positions according to Eq. (9). Inset: Retrieved speckle shift ξ_i from 1D speckle scan with i-j = 2 for the 6 diffuser positions.

4. Conclusion

A simple method based on speckle tracking has been proposed for the alignment of X-ray focusing mirrors and to remove aberrations of tilt and astigmatism. Simultaneously, the focal plane of the mirrors can be retrieved from the linearity between the tilt angle and the focal

Optics EXPRESS

length. The proposed method has been demonstrated experimentally and has shown good agreement with simulation and with measurements of the focus conducted by wire scanning techniques, but with higher accuracy and less stringent requirements on the stability of the experimental environment. Three-dimensional information can be extrapolated from the two-dimensional images, which makes it less time-consuming compared to conventional knife-edge scanning techniques. Fewer scan points are required for sufficient linear fitting than this demonstration so the method has the potential to be faster than presented here. Requiring no manual iterative procedure, the proposed method can be easily implemented as an online automatic alignment function on beamlines. With its inherent simplicity and flexibility, we believe it has the potential to be an efficient technique for alignment of X-ray optics that can be widely applied at synchrotron and laboratory-based facilities.

Acknowledgments

The work was carried out with the support of Diamond Light Source Ltd. We wish to acknowledge Andrew Malandain for support during beamtime at B16 DLS. We thank Robert Gray and Joseph Howard for sharing Zernike polynomial fitting code.

References

1. P. Kirkpatrick and A. V. Baez, "Formation of Optical Images by X-Rays," J. Opt. Soc. Am. **38**(9), 766–774 (1948).
2. H. Mimura, S. Handa, T. Kimura, H. Yumoto, D. Yamakawa, H. Yokoyama, S. Matsuyama, K. Inagaki, K. Yamamura, Y. Sano, K. Tamasaku, Y. Nishino, M. Yabashi, T. Ishikawa, and K. Yamauchi, "Breaking the 10 nm barrier in hard-X-ray focusing," Nat. Phys. **6**(2), 122–125 (2010).
3. G. E. Ice, J.-S. Chung, J. Z. Tischler, A. Lunt, and L. Assoufid, "Elliptical x-ray microprobe mirrors by differential deposition," Rev. Sci. Instrum. **71**(7), 2635–2639 (2000).
4. W. Yun, B. Lai, Z. Cai, J. Maser, D. Legnini, E. Gluskin, Z. Chen, A. A. Krasnoperova, Y. Vladimirsky, F. Cerrina, E. D. Fabrizio, and M. Gentili, "Nanometer focusing of hard x rays by phase zone plates," Rev. Sci. Instrum. **70**(5), 2238–2241 (1999).
5. W. Liu, G. E. Ice, J. Z. Tischler, A. Khounsary, C. Liu, L. Assoufid, and A. T. Macrander, "Short focal length Kirkpatrick-Baez mirrors for a hard x-ray nanoprobe," Rev. Sci. Instrum. **76**(11), 113701 (2005).
6. P. Mercère, M. Idir, P. Zeitoun, X. Levecq, G. Dovillaire, S. Bucourt, D. Douillet, K. A. Goldberg, P. P. Naulleau, and S. Rekawa, "X ray Wavefront Hartmann Sensor," AIP Conf. Proc. **705**, 819–822 (2004).
7. T. Weitkamp, B. Nöhammer, A. Diaz, C. David, and E. Ziegler, "X-ray wavefront analysis and optics characterization with a grating interferometer," Appl. Phys. Lett. **86**(5), 054101 (2005).
8. P. Mercere, S. Bucourt, G. Cauchon, D. Douillet, G. Dovillaire, K. A. Goldberg, M. Idir, X. Levecq, T. Moreno, P. P. Naulleau, S. Rekawa, and P. Zeitoun, "X-ray beam metrology and x-ray optic alignment by Hartmann wavefront sensing," Proc. SPIE **5921**, 592109 (2005).
9. P. Mercère, M. Idir, T. Moreno, G. Cauchon, G. Dovillaire, X. Levecq, L. Couvet, S. Bucourt, and P. Zeitoun, "Automatic alignment of a Kirkpatrick-Baez active optic by use of a soft-x-ray Hartmann wavefront sensor," Opt. Lett. **31**(2), 199–201 (2006).
10. M. Idir, P. Mercere, M. H. Modi, G. Dovillaire, X. Levecq, S. Bucourt, L. Escolano, and P. Sauvageot, "X-ray active mirror coupled with a Hartmann wavefront sensor," Nucl. Instrum. Methods Phys. Res. A **616**(2-3), 162–171 (2010).
11. T. D. Rolo, S. Reich, D. Karpov, S. Gasilov, D. Kunka, E. Fohtung, T. Baumbach, and A. Plech, "A Shack-Hartmann Sensor for Single-Shot Multi-Contrast Imaging with Hard X-rays," Appl. Sci. **8**(5), 737 (2018).
12. P. Mercere, M. Idir, G. Dovillaire, X. Levecq, S. Bucourt, L. Escolano, and P. Sauvageot, "Hartmann wavefront sensor and adaptive X-ray optics developments for synchrotron applications," Proc. SPIE **7803**, 780302 (2010).
13. Y. Liu, M. Seaberg, D. Zhu, J. Krzywinski, F. Seiboth, C. Hardin, D. Cocco, A. Aquila, B. Nagler, H. J. Lee, S. Boutet, Y. Feng, Y. Ding, G. Marcus, and A. Sakdinawat, "High-accuracy wavefront sensing for x-ray free electron lasers," Optica **5**(8), 967–975 (2018).
14. H. Wang, K. Sawhney, S. Berujon, E. Ziegler, S. Rutishauser, and C. David, "X-ray wavefront characterization using a rotating shearing interferometer technique," Opt. Express **19**(17), 16550–16559 (2011).
15. C. M. Kewish, M. Guizar-Sicairos, C. Liu, J. Qian, B. Shi, C. Benson, A. M. Khounsary, J. Vila-Comamala, O. Bunk, J. R. Fienup, A. T. Macrander, and L. Assoufid, "Reconstruction of an astigmatic hard X-ray beam and alignment of K-B mirrors from ptychographic coherent diffraction data," Opt. Express **18**(22), 23420–23427 (2010).
16. A. Macrander, M. Wojcik, J. Maser, N. Bouet, R. Conley, and B. Lai, "Focus of a multilayer Laue lens with an aperture of 102 microns determined by ptychography at beamline 1-BM at the Advanced Photon Source," Proc. SPIE **10389**, 1038909 (2017).
17. H. Wang, J. Sutter, and K. Sawhney, "Advanced in situ metrology for x-ray beam shaping with super precision," Opt. Express **23**(2), 1605–1614 (2015).

Optics EXPRESS

18. K. S. Morgan, D. M. Paganin, and K. K. W. Siu, "X-ray phase imaging with a paper analyzer," Appl. Phys. Lett. **100**(12), 124102 (2012).
19. S. Bérujon, E. Ziegler, R. Cerbino, and L. Peverini, "Two-Dimensional X-Ray Beam Phase Sensing," Phys. Rev. Lett. **108**(15), 158102 (2012).
20. J. P. Sutter, M. Amboage, S. Hayama, and S. Díaz-Moreno, "Geometrical and wave-optical effects on the performance of a bent-crystal dispersive X-ray spectrometer," Nucl. Instrum. Methods Phys. Res. A **621**(1-3), 627–636 (2010).
21. F. Schäfers, "The BESSY Raytrace Program RAY," in *Modern Developments in X-Ray and Neutron Optics*, A. Erko, M. Idir, T. Krist, and A. G. Michette, eds. (Springer Berlin Heidelberg, 2008), p. **24**.
22. B. Pan, K. Qian, H. Xie, and A. Asundi, "Two-dimensional digital image correlation for in-plane displacement and strain measurement: a review," Meas. Sci. Technol. **20**(6), 062001 (2009).
23. O. Hignette, A. K. Freund, E. Chinchio, P. Z. Takacs, and T. W. Tonnessen, "Incoherent x-ray mirror surface metrology," Proc. SPIE **3152**, 188–199 (1997).
24. P. P. Naulleau, P. Batson, P. Denham, D. Richardson, and J. Underwood, "An in situ scanning-slit alignment system for Kirkpatrick–Baez optics," Opt. Commun. **212**(4-6), 225–233 (2002).
25. J. C. Wyant and K. Creath, *Basic Wavefront Aberration Theory for Optical Metrology* (Academic Press, Inc., 1992).
26. M. Idir, M. Rakitin, B. Gao, J. Xue, L. Huang, and O. Chubar, "Alignment of KB mirrors with at-wavelength metrology tool simulated using SRW," Proc. SPIE **10388**, 103880Z (2017).
27. V. N. Mahajan, "Orthonormal aberration polynomials for anamorphic optical imaging systems with rectangular pupils," Appl. Opt. **49**(36), 6924–6929 (2010).
28. K. J. S. Sawhney, I. P. Dolbnya, M. K. Tiwari, L. Alianelli, S. M. Scott, G. M. Preece, U. K. Pedersen, R. D. Walton, R. Garrett, I. Gentle, K. Nugent, and S. Wilkins, "A Test Beamline on Diamond Light Source," AIP Conf. Proc. **1234**, 387–390 (2010).
29. H. Wang, Y. Kashyap, D. Laundy, and K. Sawhney, "Two-dimensional in situ metrology of X-ray mirrors using the speckle scanning technique," J. Synchrotron Radiat. **22**(4), 925–929 (2015).
30. S. Berujon, H. Wang, S. Alcock, and K. Sawhney, "At-wavelength metrology of hard X-ray mirror using near field speckle," Opt. Express **22**(6), 6438–6446 (2014).
31. V. N. Mahajan and G. M. Dai, "Orthonormal polynomials in wavefront analysis: analytical solution," J. Opt. Soc. Am. A **24**(9), 2994–3016 (2007).
32. B. Pan, H.-M. Xie, B.-Q. Xu, and F.-L. Dai, "Performance of sub-pixel registration algorithms in digital image correlation," Meas. Sci. Technol. **17**(6), 1615–1621 (2006).
33. T. Zhou, M. C. Zdora, I. Zanette, J. Romell, H. M. Hertz, and A. Burvall, "Noise analysis of speckle-based x-ray phase-contrast imaging," Opt. Lett. **41**(23), 5490–5493 (2016).

193.62.223.243 {ts '2018-10-04 05:22:00'}